TESCE ,Vol.29,No.2 pp. 49- 69

Effect of Heat Treatment on the High Temperature Oxidation Behavior of TiAl alloys

Wafaa A. Ghanem and Fathy M. Bayoumi

(Central Metallurgical Research and Development Institute)

Abstract

The Ti-51Al alloy was heat treated with different routs to study the effect of grain size and phase content on oxidation behavior in air at 750^{0}C, 850^{0}C and 950^{0}C. Oxidation mass gain of the alloys at different temperatures was measured and the corroded surface was characterized using scanning electron microscope. Parabolic oxidation kinetics was observed in most samples suggesting a diffusion limited mechanism followed , generally by a transition in oxidation kinetics to a lower rate The high temperature oxidation rate decreased by increasing the grain size of the γ matrix and increased by increasing of α_2 phase in the alloy samples. α_2 act as oxygen scavenger, this was the reason for the higher oxidation rate in the sample with 37 % α_2 . 15% α_2 in the alloy is sufficient for improving the mechanical properties and to form protective oxide film.

Keywords: High temperature – oxidation – heat treatment - TiAl alloys – mass gain

Introduction

Structural materials such as TiAl alloy system have recently attracted the attention of many researchers. TiAl alloys are regarded as very promising candidates for high temperature structural materials because of their rather high melting point, high temperature strength and low density. However , their tendency for corrosion in air and their reduced ductility at room temperature restrict their application to the high temperature structure components. Their temperature limit for high temperature

oxidation is lower than that for high temperature mechanical properties. This has become an important obstacle for these materials[1,2]. In general, a protective Al_2O_3 scale doesn't form on TiAl, particularly in air, but a scale composed of TiO_2 and Al_2O_3 forms. Such scales grow mostly parabolically with time[3-5]and consists of two or even three layers. Generally, an outer layer of finely dispersed mixture of TiO_2 and Al_2O_3 [3,4,6-8, 9]

The phase diagram of the TiAl system[10] reveals that there are two main phases can be formed in this alloy. γ phase and α_2 phase. Ti-49Al has a duplex structure ($\gamma + \alpha_2$) while Ti-51Al is a single γ phase. The controlled heat treatment can alter the microstructure hence control the mechanical properties and oxidation resistance.

Several attempts were made to develop better oxidation resistance of this alloy for example the addition of alloying elements such as molybdenum, silicon, phosphorous or niobium[11-14] . Other methods such as heat treatment, spray coating and plasma coating have been developed[15-17] .

Al_2O_3 grains are enriched near the interface between the two layers. Although they cannot be sufficiently continuous, they can act as a barrier to some degree. The rate-controlling step for steady state oxidation is ionic diffusion through the scale provided that the outer TiO_2 layer is dense. The deviation from exact parabolic kinetics is attributed to the formation of small cracks in the scale which allow gaseous diffusion of oxygen to a small degree. However, both for energy saving and environmental demands to use light materials. And since TiAl alloys are promising candidates for this purpose due to their low density and high strength at high temperature. So, this study aims to find out the effect of heat treatment on the

oxidation behavior of TiAl alloys. The effect of phase content and grain size of the α_2 phase will be studed at different temperature 750^0C, 850^0C and 950^0C

Experimental

Materials

The Ti-Al alloys used in this investigation were kindly provided by Kobe Steel Co. Japan. The chemical composition of the different alloy samples are shown in Table 1. The alloys were prepared by argon arc melting with a non-consumable tungsten electrode, using high purity titanium and aluminum chips (99.9% Ti and 99.9% Al), to make a 100g button ingot. The chemical compositions of the ingot were determined by X-ray Florescence, type ARL 9400, Switzerland. For heat treatment, samples were cut from the button ingot and wrapped with tantalum foil. They were heat treated in a vertical furnace equipped with a vacuum system under high purity argon. Prior to heat treatment, the furnace was evacuated to 5×10^{-3} Pa, and then backfilled with argon. The temperature was monitored by a Pt/Pt-Rh thermocouple held next to the samples. After aging, the samples were furnace cooled. The routs for heat treatment are listed in Table 2

Microstructures were examined by Nomaraski-type optical microscopy. For microstructure examinations the samples were etched with 2% HF, 5% H_3PO_4 etchant

Table 1 The chemical composition of the alloy samples

Samples	Ti	Al	N	O	H	Si	Mn	Cr
1 (as received)	Bal.	51.0	0.004	0.114	0.003	<0.01	0.02	<0.01
2	Bal.	49.0	0.0057	0.115	0.001	<0.01	0.021	<0.01

Table 2 Heat treatment of the alloys

No.	Main composition	Heat treatment
1a	Ti-51Al	Heated to 1365^{0}C for 30 minutes and furnace cooled
1b	Ti-51Al	Heated to 1365^{0}C for 3 minutes and furnace cooled
1c	Ti-51Al	Heated to 1150^{0}C for 60 minutes and furnace cooled
1d	Ti-51Al	Heated to 1200^{0}C for 60 minutes and furnace cooled
1e	Ti-51Al	Heated to 1200^{0}C for 10 hours and furnace cooled
2	Ti-49Al	Heated to 1435^{0}C for 5 minutes and furnace cooled

Corrosion testing

The isothermal oxidation tests for the alloys at different temperatures in air were measured using thermogravemetric system described in earlier publication[9]. The samples were placed inside the furnace after the temperature of the furnace reaches the equilibrium value of the test ± 2-3 ^{0}C. the temperature is regulated using Heraeus temperature control system, Germany. This uses Pt/Pt-Rh thermocouple which is placed in the furnace at the hot zone where the sample is hanged. The furnace is switched on and left almost for 30 minutes before placing the sample to ensure the equilibrium temperature has reached. Specimens, prior to oxidation tests,

were cut from the ingots in the form of 3 mm thick discs, polished using 1000 grit SiC paper and ultrasonically cleaned in acetone.

The mass gain was measured for samples exposed to air at various temperatures (750 - 950^{0}C) for different time intervals, up to 500 hrs.

. The samples were used in duplicates for taking the average and hanged using nichrome wire at the heat affected zone of the furnace. This wire is connected to digital sensitive balance at the times of each test.

The morphology of the corroded surface was examined using an SEM model JEOL-JSM.T20, Japan. Microstructure and optical micrographs were examined by Nomarski-type optical microscopy

Results and Discussions

Effect of heat treatment

Table 3 list the results of heat treatment (phases and grain size) of alloys 2 and 3

Table 3 Phases and grain size of the heat treated alloys

Alloy No.	Phases	Grain size
1a	α_2 37% + γ 63%	55 μm
1b	α_2 15% + γ 85 %	60 μm
1c	γ 100%	55 μm
1d	γ 100%	70 μm
1e	γ 100%	130 μm
2	α_2 25% + γ 75%	430 μm

Microstructure of the heat treated samples

- The micro structure shows striped clusters of ultra-fine γ grains. The grains grow at 1200C, >20h (1300C, >2h) to become equiaxed γ grains (see photo (Ti-49Al; 1200C x 24h F/C). (see Fig.2)
- α_2 phase appears in 1a and 1b which is preferentially precipitated along the γ grains in the stripped clusters. (see Fig.3)

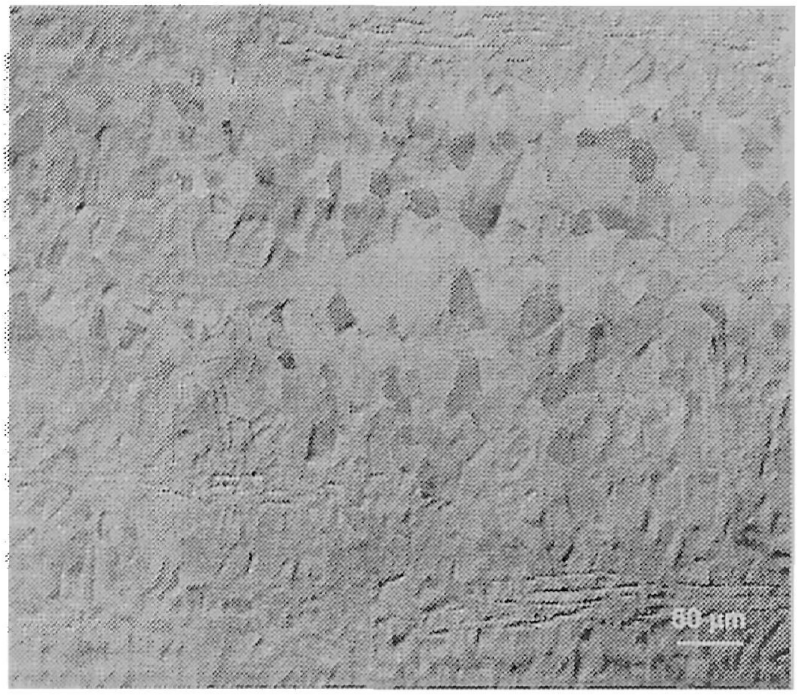

Fig. 1 Microstructure of the as-received Ti-51Al alloy (γ G.S. 20 µm)

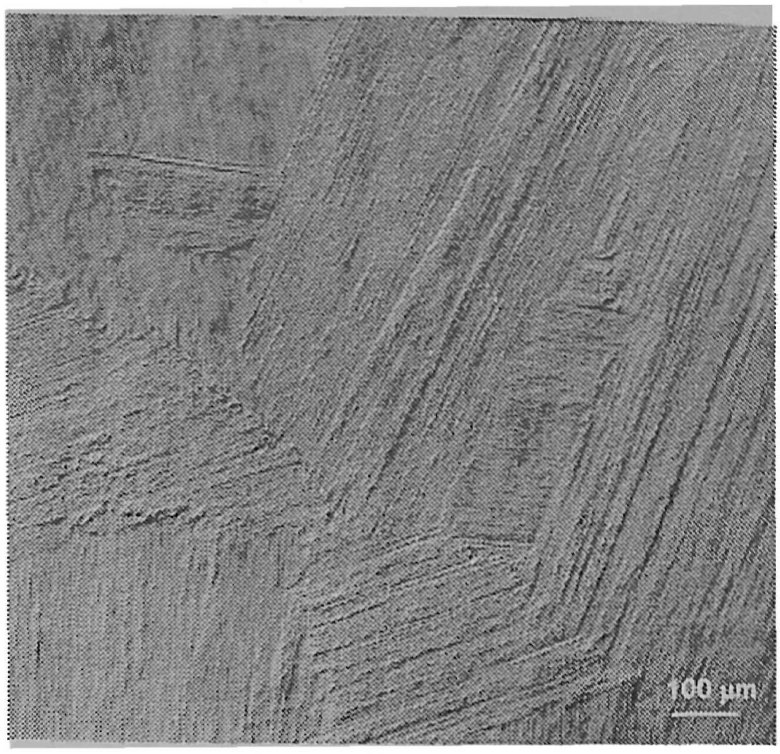

Fig. 2 Microstructure of Ti-49Al alloy heat treated at 1435^{0}C for 5 minutes and furnace cooled colony size 430 µm , α_2 = 25%.

(1a)

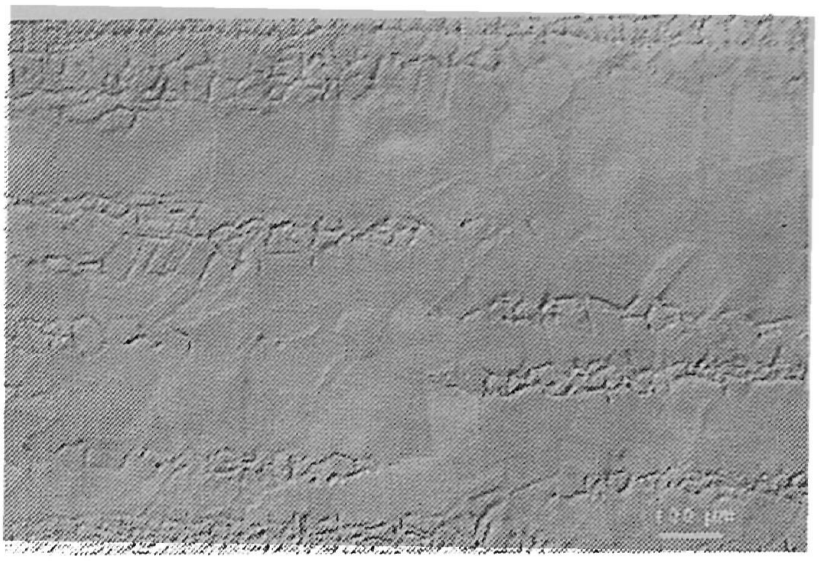

(1b)

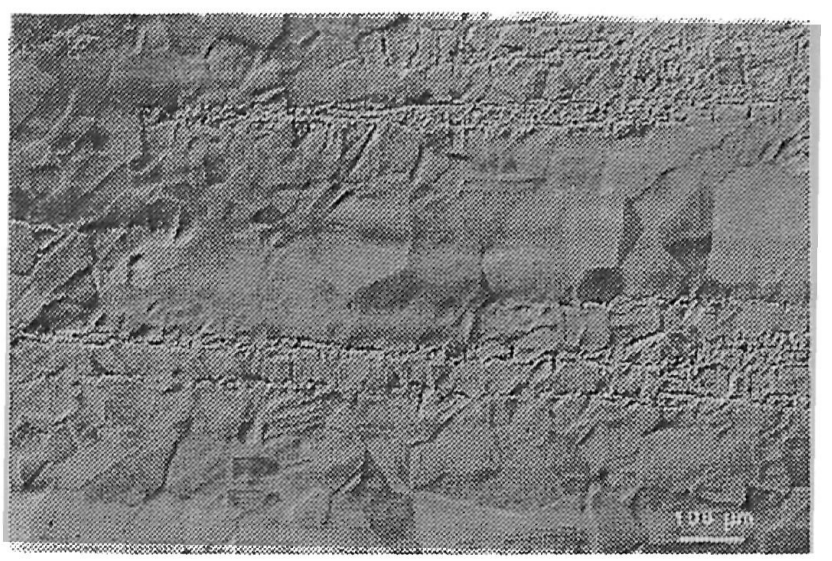

Fig. 3 Microstructure of Ti-51Al alloy heat-treated at 1365^0C

(1a) , for 30 minutes and furnace cooled (α_2 = 37%).

(1b) , for 3 minutes and furnace cooled (α_2 = 15%).

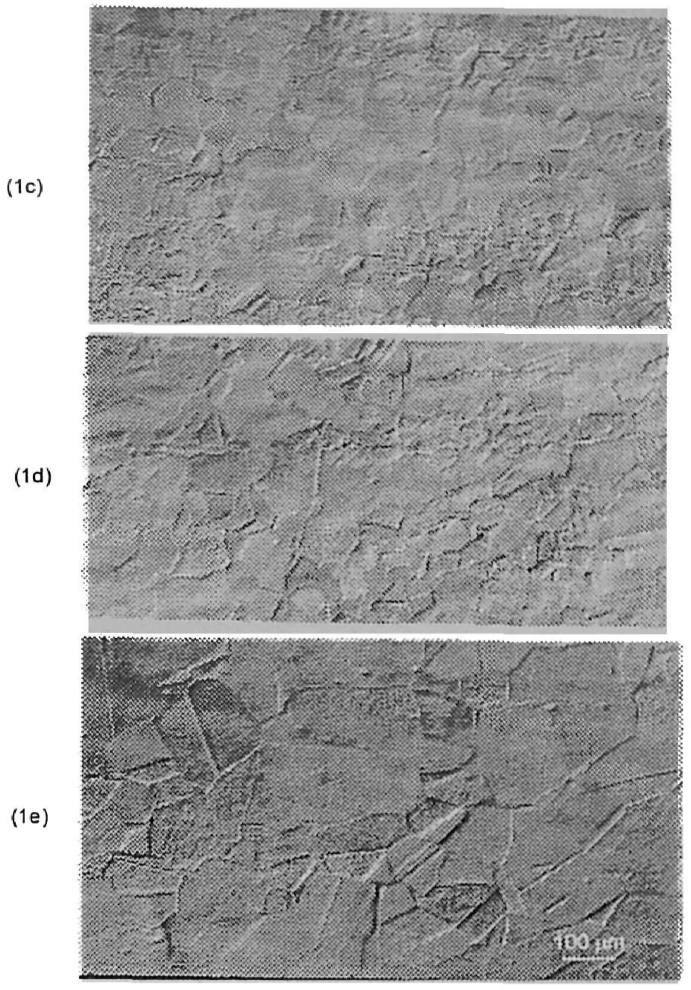

Fig. 4. Microstructure of the Ti-51Al alloy heat treated and furnace cooled

(1c): at 1150^{0}C for 1 hr, (γ G.S. 55 µm)

(1d): at 1200^{0}C for 1 hr, (γ G.S. 70 µm)

(1e): at 1200^{0}C for 1 hr, (γ G.S. 130 µm)

Effect of the phase content.

Fig. 5 shows the variation, with oxidation time, of the mass gain of the Ti-51Al, after heat treatment leading to different contents of α_2 phase, at 750^{0}C. Generally the mass gain increases with time. A transition in oxidation kinetics was observed for samples with 0 % α_2 (as received (1)) and with 37% α_2 (2b). The curves in the as received (1) and in 2b samples showed linear oxidation kinetics at the beginning of the oxidation reaction i.e.

$$\frac{d\ln(mass\ gain)}{d\ln(time)} \approx 0.95 \qquad (1)$$

After about 100 hrs the oxidation kinetics showed almost a parabolic behavior;

$$\frac{d\ln(mass\ gain)}{d\ln(time)} \approx 0.5 \qquad (2)$$

This means that the mechanism of oxidation has become diffusion controlled i.e. a protective film has been formed. For sample 1b where the % of α_2 is 15 % the oxidation kinetics is almost one line with gradient 0.5 i.e. parabolic kinetics;

The as received sample having γ single phase with grain size 20 μm is the best in corrosion resistance as its steady state is parabolic while it has the least oxidation rate constant. However this sample has low ductility at room temperature which makes it difficult to be fabricated consequently limits its use. One way to improve its ductility and also mechanical properties in general is by heat treatment to convert it from γ single phase into the duplex structure with several % α_2 phase [18-20]. According to these results the sample with 15 % α_2 satisfies both requirements i.e. mechanical properties as well as the acceptable oxidation resistance. The oxidation resistance is proven from its tendency for parabolic behavior where;

Increasing the temperature to 850^{0}C, increased the the oxidation rate constant for all samples. But a transition to parabolic behavior is observed for the samples 1 and 1b. Sample 1a, with 37% α_2, shows the greatest oxidation rate. However , the oxidation rate increase, generally, by increasing the α_2 content. α_2 phase was proven [21-23] to be oxygen scavenger this increase the tendency for inward diffusion of oxygen and consequently possible internal oxidation which is responsible for the higher oxidation rate. Presence of 15% α_2, still able to protect the surface where a diffusion barrier oxide film is formed at the same time is good in mechanical properties.

At 950^{0}C the general trend is the same but higher oxidation rate constant is obtained. Samples 1 and 1a showed transition corrosion kinetics to parabolic behavior but, at this high temperature, sample 1b (15% α_2) shows the slowest mass gain growth rate in its second stage kinetics (stage (II) on Fig. 7). At the time , sample 1a (with 37% α_2) still shows greater tendency for higher rate of oxidation where;

$$\frac{d\ln(mass\ gain)}{d\ln(time)} \approx 0.8 \qquad (3)$$

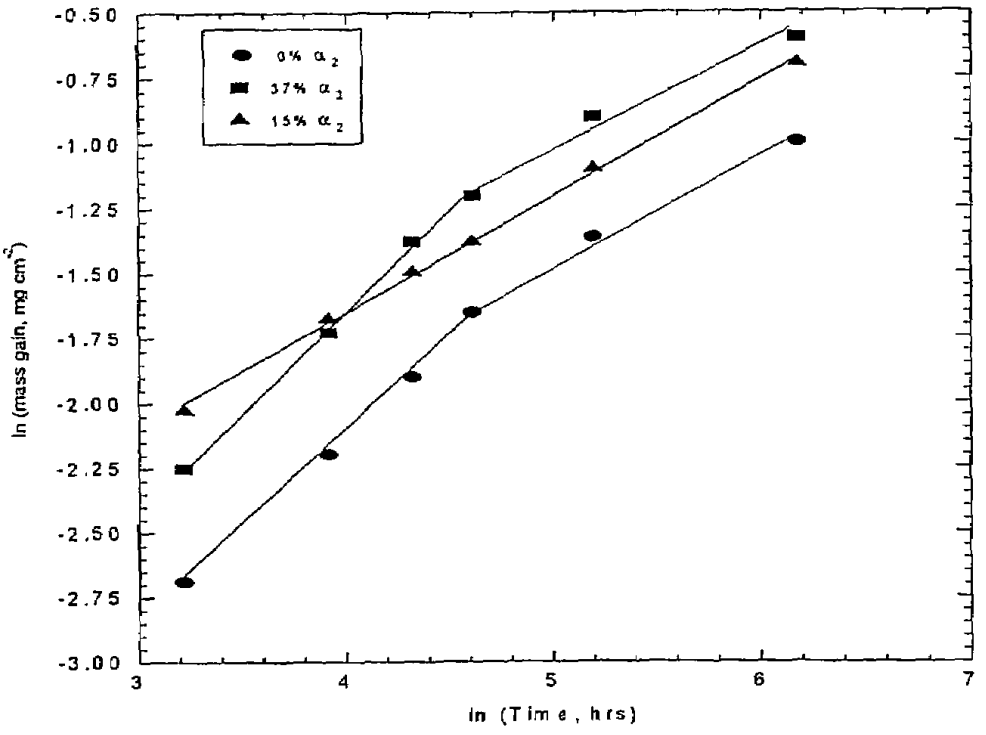

Fig.5 Variation with time of oxidation of Ti-51Al alloy at 750^{0}C, with various contents of γ phase

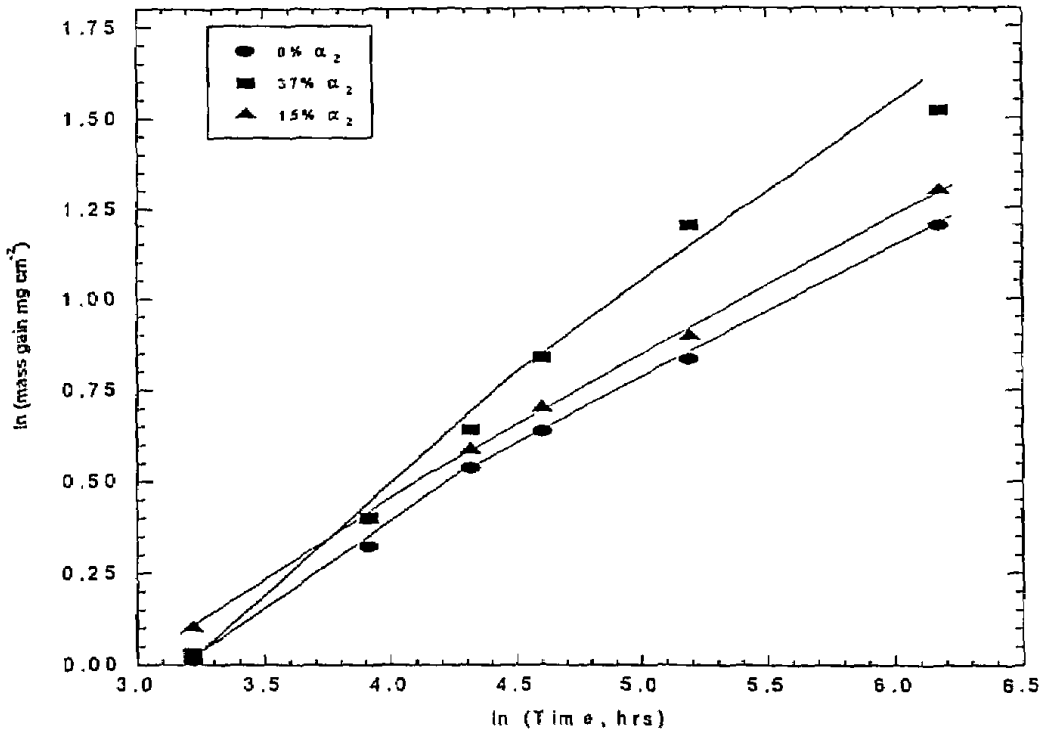

Fig.6 Variation of mass gain with time of oxidation of Ti-51Al alloy at 850^{0}C with various contents of γ phase.

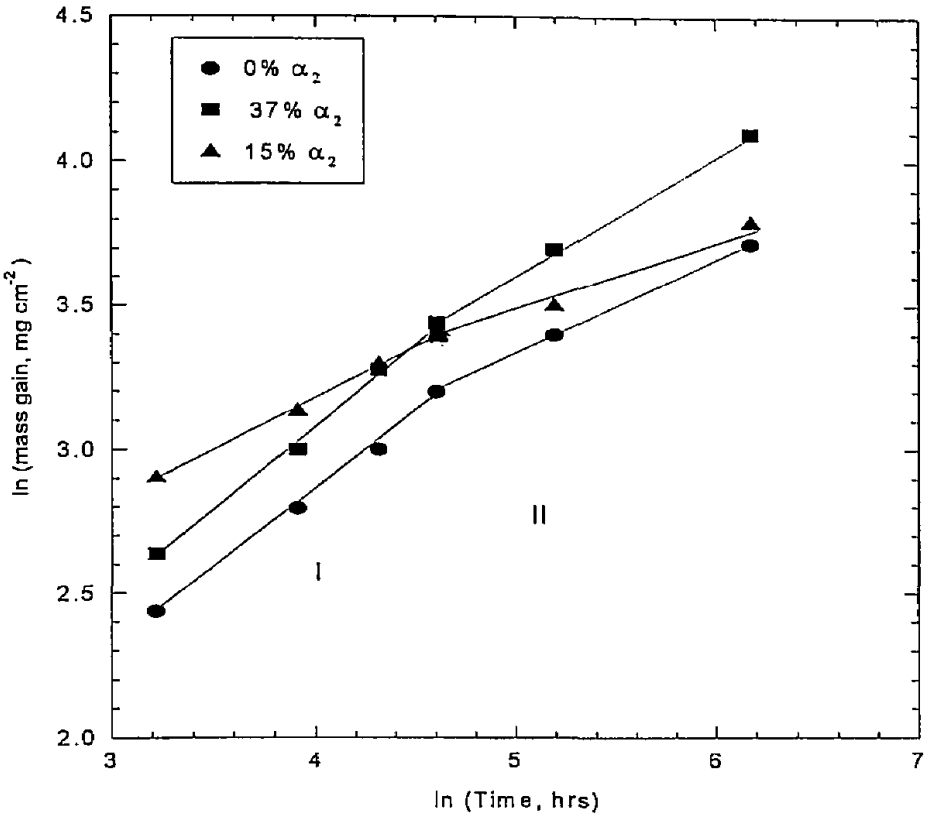

Fig.7 Variation of mass gain with time of oxidation for Ti-51Al alloy at 950^{0}C, with various % of α_2 in γ phase matrix.

Fig. 8 shows scanning electron micrograph for the alloys 1a and 1b with 37% and 15% α_2 respectively. It is clear that the sample with high α_2 % shows more roughening of the surface than the sample with less α_2 %.

(1a)

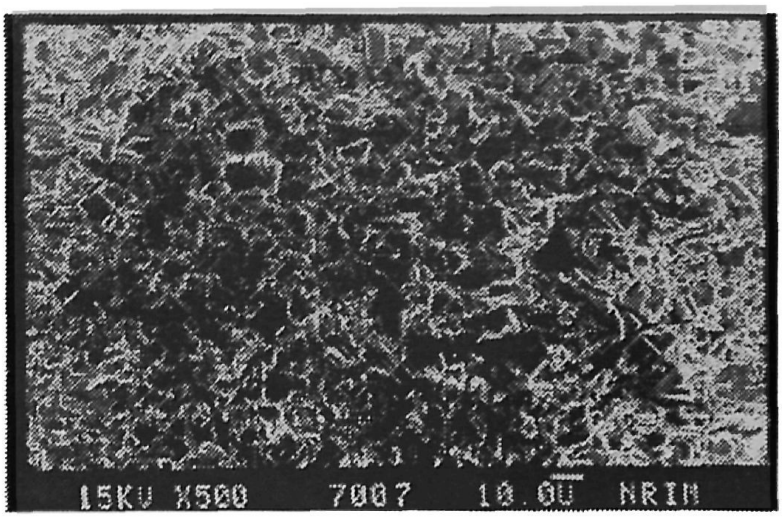

(1b)

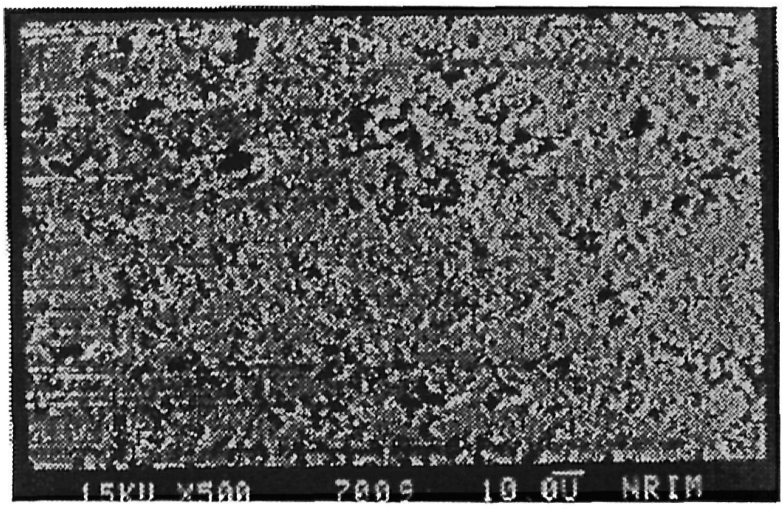

Fig. 8 SEM micrographs for alloys 1a and 1b corroded in air at 950^{0}C for 100 hrs.

Effect of the grain size:

Fig. 9 shows the variation, with oxidation time, of the mass gain in air at 750^{0}C with different grain size of the single γ phase Ti-51Al. The mass gain, generally, increases parabolically with time revealing diffusional limited kinetics. It can be, also, be

observed that the oxidation kinetics rate constant increase by increasing the grain size of the Ti-51Al.

As the oxidation at high temperature proceeds, some authors observed phase transition occurs at some depth under the surface for some alloys including TiAl alloys[24-26] , it is also observed in our findings[9] . In case of TiAl alloys, this transformation is attributed to the outward diffusion of Al. Al depletes more than Ti

$$1\ 1/3\ Al + O_2 \rightarrow 2/3\ Al_2O_3 \quad (4)$$

$$Ti + O_2 \rightarrow TiO_2 \quad (5)$$

The formation of this subsurface phase can result in the following problems[26];

1. Degrade both the toughness and the ductility of the alloy, especially at low temperatures.
2. Reduce corrosion resistance
3. Cause distortion or even rupture due to resulting internal stresses.

So, α_2 phase is formed under the surface as the oxidation proceeds. Mutoh et al[27] State that where positive and negative change of concentration in Ti and Al were observed in a given depth from the specimen surface, Ti_3Al (α_2 phase) is formed not only beneath the surface film but also along the grain boundaries in the specimen interior for exposure times up to 500 hrs. Misra[28] showed that oxygen in the α_2 phase changed positively , and this phenomena is now known as one of the examples of the scavenging effect of the α_2 phase. So , it can be concluded that, as the grain size increases the possibility to form α_2 phase is greater, and since α_2 phase was proven to act as oxygen scavenger, so this explains why the rate of oxidation increase as the grain size increase.

Transition in oxidation kinetics is almost observable.

Fig. 10 shows the variation of the mass gain with oxidation time of the heat treated Ti-51Al alloys with different grain size in air at 850^0C. Generally the kinetics shows parabolic behavior followed by a transition to lower slopes.

$$\frac{d\ln(mass\ gain)}{d\ln(time)} \approx 0.5$$

The parabolic rate constant increases as the grain size and the temperature increase.

Fig. 11 shows the variation of the mass gain with for heat treated Ti-51Al with different grain size oxidized in air at 950^0C. The kinetics generally follows parabolic behavior and the rate constant increased by increasing temperature and by increasing the grain size.

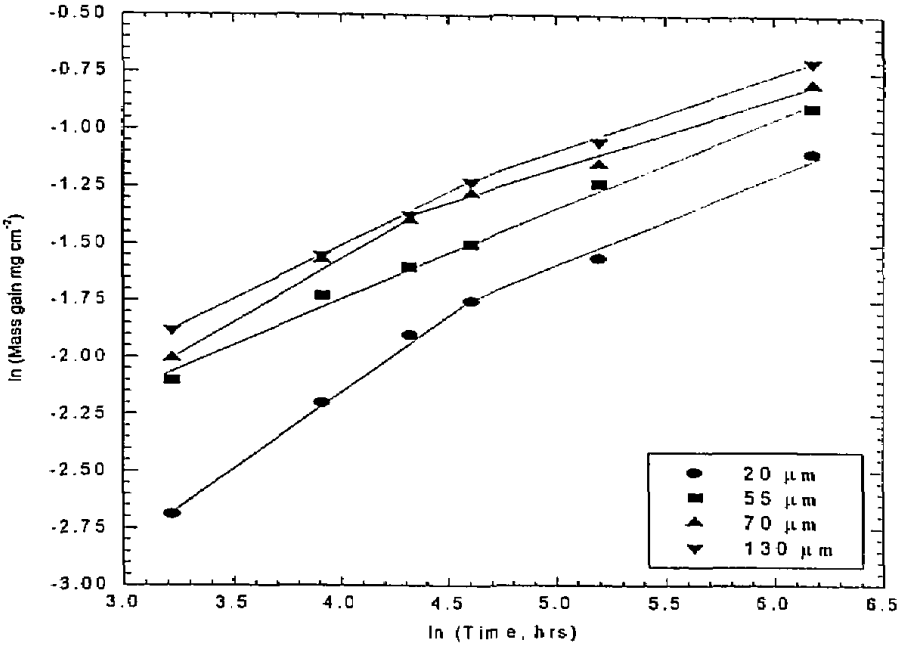

Fig.9 Variation, with time of oxidation, of the mass gain in air at 750^{0}C, for alloys with different grain size of the γ phase.

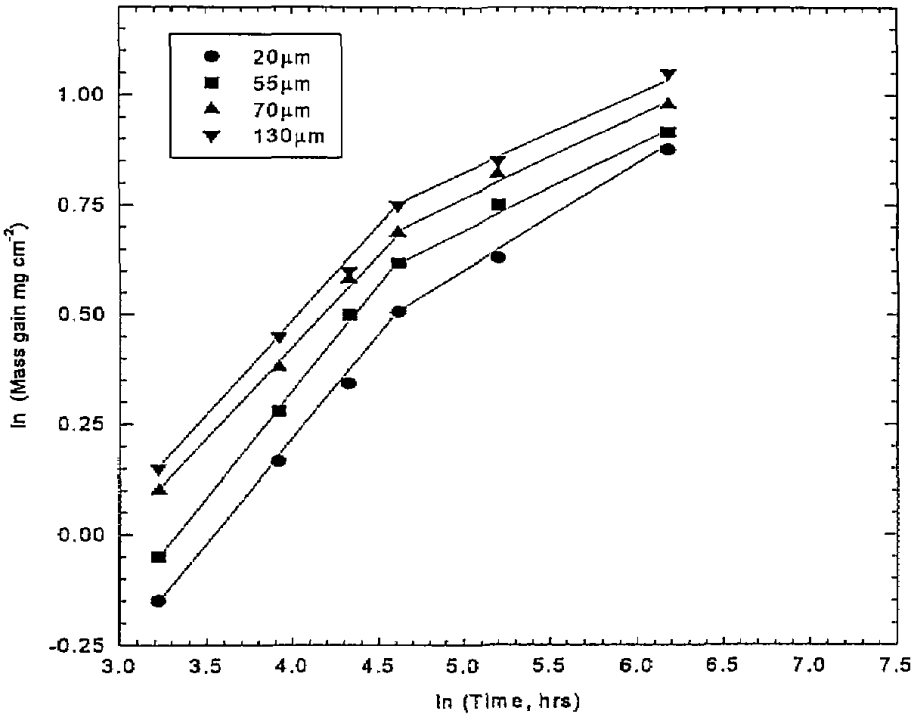

Fig.10 Variation, with time of oxidation, of the mass gain in air at 850^{0}C, for alloys with different grain size of the γ phase.

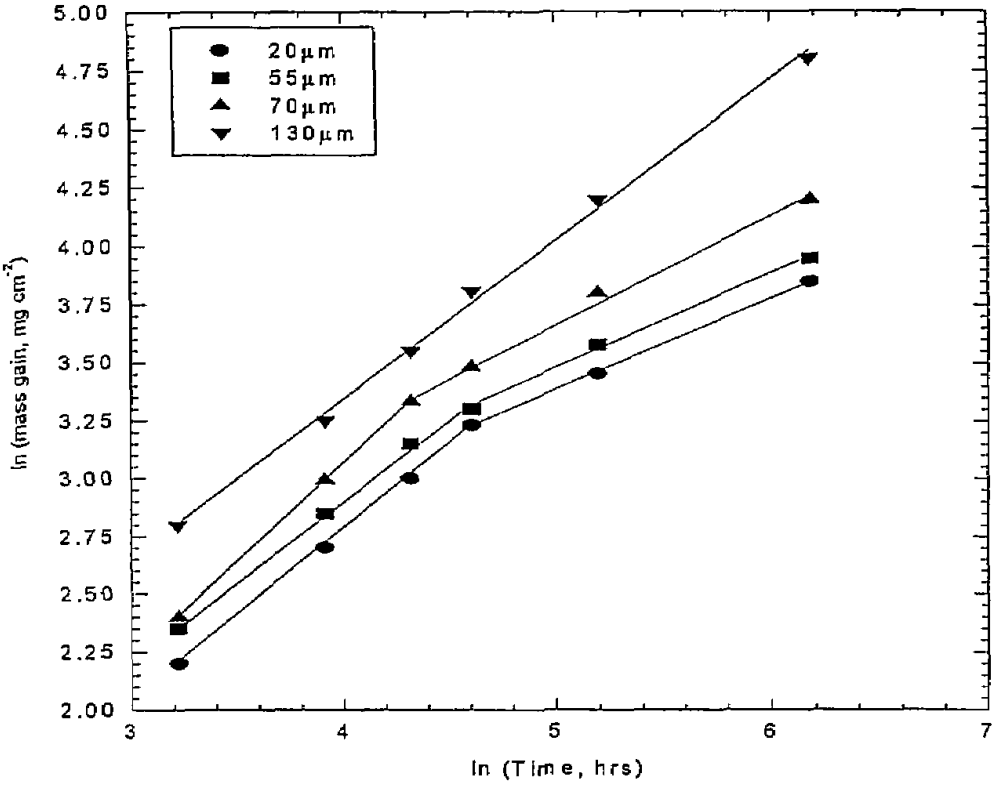

Fig.11 Variation, with time of oxidation, of the mass gain in air at 950 ^{0}C, for alloys with different grain size of the γ phase.

Conclusions

1. As the α_2 phase increase, the rate of corrosion increases because this phase acts as oxygen scavenger.
2. Phase transition occurs due to corrosion at high temperature for subsurface α_2 phase.
3. α_2 phase preferably precipitate on the grain boundary, this explains why the corrosion rate increase as the grain size increase.
4. By controlled heat treatment, the factors that control the tensile and corrosion can be compromised and must be considered parallel.

Acknowledgment

The authors express their thanks and gratitude to all members in National Research Institute of Metals (NRIM), Japan for providing facilities for several measurements and valuable discussions specially Prof. Dr. Tanabe. Greatest thanks also are to Dr. B. G. Ateya for valuable discussions

References

1. M. Takeyama, Mater. Sci. and Engn., A152, 269 (1992)
2. S.C. Huang, Structural Intermetallics. In: R. Darolia et al., editors. Warrendale, PA: The Minerals, Metals and Materials Society, 299-307 (1993).
3. S. Becker, A. Rahmel, M. Schorr and M. Schütze, Oxid. Met., 38, 425 (1992).
4. G. H. Meier, D Appalonia, R. A. Perkins and K. T. Chiang, In: T. Grobstein and J. Doychak, editors. Oxidation of High Temperature Intermetallics, Warrendale, PA, USA: TMS, p. 185. (1988)
5. E. U. Lee and H. Waldman, Scripta Metall. 22, 1389 (1988)
6. K. Kasahara, K. Hashimoto, H. Doi, and T. Tsujimoto, J. Jpn. Inst. Met. 53, 58 (1989).
7. N. S. Choudhury, H. G. Graham, and J. W. Hinze, in Properties of High Temperature Alloys with Emphasis on Environmental Effects, Z. A. Foroulis and F. S. Pettit, eds., The Electrochemical Society, Princeton, p. 668 (1976).
8. E. Kobayashi, M. Yoshihara, and R. Tanaka, High Temp. Technol. 8, 179 (1990).
9. Wafaa A. Ghanem and Fathy M. Bayoumi, Al-Azhar Bulletin of Science, in press
10. Binary Alloy Phase Diagrams, T. B. Massalski ed., ASM, (1986).

11. R. A. Perkins, K. T. Chiang, and G. H. Meier, Scripta Metall. 21, 1505 (1987)

12. T.T. Cheng, M. R. Willis and I. P. Jones, Intermetallics, 7, pp.89-99 (1999)

13. Y. Norio, K. Takuro, Y. Takayuki and O. Osamu, Mater. Trans. V 43, pp. 3211-3216 (2002)

14. A. Donchev, B. Gleeson and M. Schutze, Intermetallics, v 11, n 5,pp. 387-398 (2003).

15. H. Anada and Y. Shida, J. Jpn. Inst. Metals, 58, pp. 746-753 (1994).

16. W.Fang, H. S. Ko, H. Hashimoto, T. Abe and H. Y. Park, Mater. Sci. and Eng. A. v 329-331, pp. 708-712 (2002).

17. M. Yoshihara, S. Taniguchi and C. Y. Zhu, Mater. Sci. Forum, v 369-372, pp. 395-402 (2001)

18. M. Takeyama, Mater. Sci. and Engn., A152, 269 (1992)

19. T. Kumagai, E. Abe, T. Kimura and M. Nakamura, Scripta Materialia, vol. 34, No. 2, pp. 235-242, 1996.

20. T. Kumagai, E. Abe, M. Takeyama and M. Nakamura, Mat. Res. Soc. Symp. Proc. 364, 181 (1995).

21. R. Uemori, T. Hanamura and H. Morikawa, Scripta Metall. Mater. 26, p. 969 (1992).

22. A. Denquin, S. Naka, A. Huguet and A. Menand, Scripta Metall. Mater. 28, p. 1131 (1993).

23. K. Hono, E. Abe, T. Kumagai and H. Harada, Scripta Metall. Mater. 35, p. 495-499 (1996).

24. N. Zheng, W. Fischer, H. Grübmeier, V. Shemet, W. J. Quadakkers, Scripta Metall. Mater. 33, p. 47-53 (1995).

25. Y. F. Cheng, F. Dettenwanger, J. Mayer, E. Schumann and M. Rühle, Scripta Mater, 34, p. 707-711 (1996).

26. D. J. Young and B. Gleeson, Corros. Scie. 44, p. 345-357 (2002).

27. I. Mutoh, K. Homma, T. Tanabe and M. Nakamura, J. Nuclear Mater. 231 p. 132-140 (1996).

28. A. K. Misra, Metall. Trans. A 22A, p. 715 (1991).